

Fermi-surface collapse and dynamical scaling near a quantum critical point

Sven Friedemann^{*}, Niels Oeschler^{*}, Steffen Wirth^{*}, Cornelius Krellner^{*}, Christoph Geibel^{*}, Frank Steglich^{*}, Silke Paschen[†], Stefan Kirchner[‡], and Qimiao Si[‡]

^{*}Max Planck Institute for Chemical Physics of Solids, Nöthnitzer Str. 40, 01187 Dresden, Germany, [†]Institute of Solid State Physics, TU Vienna, Wiedner Hauptstr. 8-10, 1040 Vienna, Austria, [‡]Department of Physics and Astronomy, Rice University, Houston, Texas 77005-1892, USA, and [§]Max Planck Institute for the Physics of Complex Systems, Nöthnitzer Str. 38, 01187 Dresden, Germany

Submitted to Proceedings of the National Academy of Sciences of the United States of America

Classification: Physical Sciences—Physics

Quantum criticality arises when a macroscopic phase of matter undergoes a continuous transformation at zero temperature. While the collective fluctuations at quantum critical points are being increasingly recognized as playing an important role in a wide range of quantum materials, the nature of the underlying quantum critical excitations remains poorly understood. Here we report in-depth measurements of the Hall effect in the heavy-fermion metal YbRh₂Si₂, a prototypical system for quantum criticality. We isolate a rapid crossover of the isothermal Hall coefficient clearly connected to the quantum critical point from a smooth background contribution; the latter exists away from the QCP and is only detectable through our studies over a wide range of magnetic field. Importantly, the width of the critical crossover is proportional to temperature, which violates the predictions of conventional theory and is instead consistent with an energy over temperature, E/T , scaling of the quantum critical single-electron fluctuation spectrum. Our results provide evidence that the quantum-dynamical scaling and a critical Kondo breakdown simultaneously operate in the same material. Correspondingly, we infer that macroscopic scale-invariant fluctuations emerge from the microscopic many-body excitations associated with a collapsing Fermi surface. This insight is expected to be relevant to the unconventional finite-temperature behavior in a broad range of strongly correlated quantum systems.

Quantum critical point | YbRh₂Si₂ | Hall effect | dynamical scaling

Quantum criticality, epitomizes the richness of quantum effects in macroscopic settings [1]. The traditional description is based on the framework of Ginzburg and Landau [2], which focuses on the notion of an order parameter, a classical variable. The order parameter delineates the symmetry breaking of the macroscopic phases, while its fluctuations at ever-increasing length and time scales characterize the approach towards a second-order quantum phase transition. For metallic antiferromagnets, this theory appears in the form of a spin-density-wave quantum critical point (QCP) [3, 4]. Here, the macroscopic fluctuations of the order parameter are described by a Gaussian theory at the fixed point, with a vanishing effective coupling among the collective modes in the zero-temperature ($T = 0$), zero-energy ($E = 0$) and infinite-length limit. Consequently [5], the collective fluctuations will violate E/T -scaling.

By contrast, an unconventional class of quantum criticality, emerging from studies in recent years [1], incorporates not only the slow fluctuations of the order parameter, but also some inherent quantum modes. For heavy-fermion metals, the new quantum modes are associated with a critical breakdown of the Kondo screening effect and the concomitant single-electron Kondo resonance excitations [6, 7, 8]. These new critical modes can lead to a critical field theory that is interacting, instead of Gaussian, and the collective fluctuations will satisfy E/T -scaling [9, 10]. The critical Kondo effect itself is manifested in the nature of microscopic single-electron

excitations, with the Fermi surface undergoing a severe reconstruction at the QCP.

To date, there has been no experiment to determine that the critical Kondo destruction is the underlying mechanism for the dynamical E/T -scaling. In the heavy-fermion quantum critical material CeCu_{5.9}Au_{0.1}, the magnetic dynamics have been shown to display such a scaling [9]. In this material, however, the unconventional QCP appears only by tuning of chemical doping or pressure [11]; consequently it has so far not been possible to probe its Fermi surface and related single-electron properties with sufficient resolution. The heavy-fermion system YbRh₂Si₂ features an unconventional QCP that is accessible by the application of a relatively small magnetic field [12, 13], thereby allowing the study of magnetotransport across the QCP. While indications of a rapid Fermi surface change in YbRh₂Si₂ has appeared through the observation of a crossover in the Hall effect [14], no information has been extracted on the dynamical fluctuation spectra of either the magnetic or single-electron excitations. Moreover, the Hall crossover has alternatively been interpreted in terms of a background contribution in the non-magnetic heavy-fermion phase through either minute valence variations [15] or Zeeman splitting of the bands [16, 17], leaving the nature of the quantum critical single-electron excitations uncertain. In addition, the observation of sample dependences in the low-temperature Hall coefficient raises the important question of how these affect the Hall crossover [18]. To resolve these fundamental issues, we carry out comprehensive, in-depth Hall-effect measurements over a wide range of the control parameter, the magnetic field, down to very low temperatures. We establish a sample-dependent background component of the Hall crossover, which in turn allows us to isolate a critical component of the crossover with properties that are sample-independent. In addition, we identify a robustly linear-temperature width of the critical Hall crossover, which is compatible with a quantum-dynamical scaling of the critical single-electron excitations. Our findings lead to an unexpectedly direct linkage between the scale-invariant macroscopic fluctuations and the microscopic physics of a collapsing Fermi surface.

Results

We study the magnetotransport in tetragonal YbRh₂Si₂ using a crossed-field setup, in which two external magnetic fields are applied in perpendicular directions. This separation allows for a disentanglement between field-tuning of ground states through B_2 and generation of Hall response through B_1 : One field, B_1 , along the magnetic hard c axis and perpendicular to the electrical current, is used to extract the initial slope of the Hall resistivity, ρ_H , *i.e.* the linear-response Hall coefficient, R_H (see Supplementary Information I). The second field, B_2 , applied within the magnetically easy ab plane and along the current direction, is used as the control parameter

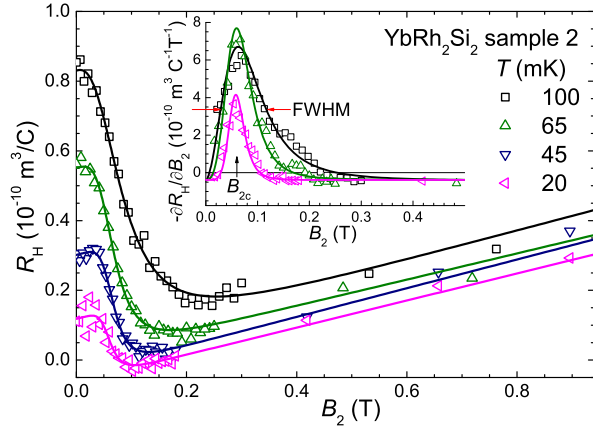


Fig. 1. Crossed-field Hall-effect results of YbRh₂Si₂. Selected isotherms of the initial-slope Hall coefficient R_H as a function of B_2 for sample 2 [which has the smallest residual resistivity (cf. Supplementary Information II)]. The solid lines are best fits of the empirical crossover function given in eq. 5 in the Methods section, extending up to 2 T. The anomalous contribution to the Hall effect can be neglected as explained in the Supplementary Information III. The inset illustrates the decomposition of the crossover in $R_H(B_2)$ into the critical and background components. Here, $-\partial R_H(B_2)/\partial B_2$ is plotted as a function of B_2 together with the derivatives of the fitted functions (solid lines). The background crossover term corresponds to the non-zero constant offset. The critical crossover term is represented by the sharp peak near B_{2c} (marked by vertical arrow), whose full-width at half-maximum, FWHM, is defined as the crossover width (specified for one temperature by the red horizontal arrows). Standard errors of R_H are typically of the size of the symbols.

that tunes the system from an antiferromagnetic ground state at low fields across the QCP towards a high-field paramagnetic state. The adjacent phases on both sides of the QCP obey Fermi liquid properties, like a quadratic temperature dependence of the resistivity [13]. We consider two samples, which span the whole range of sample dependences in the Hall coefficient (see Supplementary Information II).

Figure 1 shows the isothermal linear-response Hall coefficient of our highest-quality sample as a function of B_2 . Two features are evident. First, for B_2 much larger than the quan-

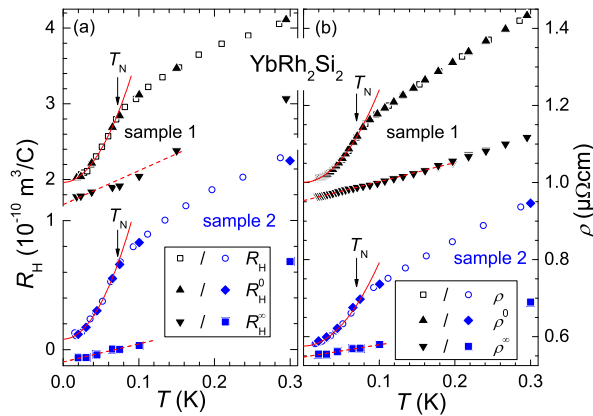


Fig. 2. Limiting values of the Hall and magnetoresistivity crossover. (a) Fit parameters R_H^0 and R_H^∞ of the crossover in R_H plotted for sample 1 and sample 2 as a function of temperature together with the measured initial-slope Hall coefficient R_H . The residual resistance ratios are 70 and 120 for sample 1 and sample 2, respectively. (b) Corresponding quantities ρ^0 and ρ^∞ from the analogous analysis of the magnetoresistivity crossover (see Supplementary Information IV). Solid lines correspond to fits of a quadratic temperature dependence below T_N (see Supplementary Information V), as already observed previously for $\rho(T)$ [13]. Dashed lines are guides to the eye. Arrows indicate the Néel temperature. Standard deviations are smaller than the symbol size.

tum critical field, B_{2c} , the Hall coefficient shows a sizable variation with the magnetic field; within the experimental error it is linear in B_2 . This background feature is likely due to Zeeman splitting [17] since no indication for a valence change [15] has been observed. The identification of this background feature is only possible because we have measured in a substantially extended range of B_2 (see Supplementary Information I). Second, there is a sharp crossover feature that rides on top of the background contribution. This sharp feature is located near B_{2c} , and will henceforth be termed the critical Hall-crossover component.

The inset of Fig. 1 further illustrates the systematic decomposition of the Hall crossover into the background and critical components. It plots $-\partial R_H/\partial B_2$ as a function of B_2 . The background term appears as an underlying non-zero offset, while the critical term manifests itself as a sharp peak near B_{2c} . More quantitatively, Fig. 1 shows the separation of the two components using a fitting procedure specified in the Methods section.

The critical component is characterized by the difference between R_H^0 , the Hall coefficient before the crossover, and R_H^∞ , the Hall coefficient after the crossover. The temperature dependence of R_H^0 and R_H^∞ in the low- T range for both samples is shown in Fig. 2(a). The experimental finding of a pronounced quadratic temperature dependence of R_H^0 below T_N allows a proper extrapolation to $T \rightarrow 0$ yielding a *finite difference* between R_H^0 and R_H^∞ persisting to zero temperature (see Supplementary Information V). This difference is naturally associated with a change of the Fermi surface. The *magnitudes* of R_H^0 and R_H^∞ , on the other hand, are different for the different samples rendering the sample dependences of the Hall coefficient a common property of the two phases at either side of the QCP. Recent *ab initio* calculations of the Hall coefficient in YbRh₂Si₂ suggest that these sample depen-

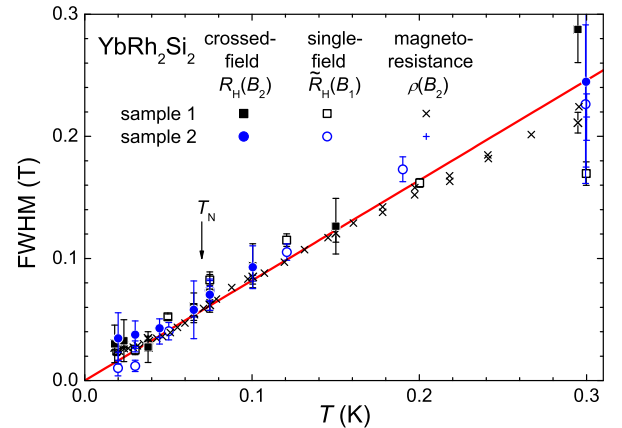


Fig. 3. Full-width at half-maximum, FWHM, of the Hall crossover. The width was determined from the derivatives of the fits to $R_H(B_2)$ in the crossed-field setup, to the simultaneously measured magnetoresistivity $\rho(B_2)$, and to $\tilde{R}_H(B_1)$ of the single-field experiment, respectively. See inset of Fig. 1 for the definition of the FWHM. The values for $\tilde{R}_H(B_1)$ were scaled by $1/11 = B_{2c}/B_{1c}$ (Ref. [13]) to account for the c axis vs. ab plane magnetic anisotropy of YbRh₂Si₂. The solid line represents a linear fit to all data sets with the magnetoresistivity data being well described up to 1 K, see Fig. S6 in the Supplementary Information. Within the experimental accuracy this fit intersects the ordinate at the origin. Where there is overlap, our magnetoresistivity results are in good agreement with the FWHM directly extracted from the derivative of $\rho(B_2)$ presented in Ref. [20]. The crossed-field data obtained earlier in a very limited temperature range [14] are in good agreement with both our results and the linear fit. The different temperature dependence found earlier was dominated by the former single-field results differing from ours. This difference is likely a result of an improved orientation procedure that only became possible in a new setup (see Supplementary Information I). Arrow indicates the Néel temperature. Error bars are standard deviations.

dences are the effect of multiple Fermi surface sheets. The "small" (4f-core) and "large" (4f-itinerant) Fermi surfaces at fields below and above B_{2c} in YbRh_2Si_2 are respectively dominated by two hole and one hole/one electron Fermi surface sheets [19]. Correspondingly, the step of R_H as B_2 increases through B_{2c} is expected to be negative, as is indeed seen here.

By contrast, the crossover position and the crossover width of the critical component show essentially no sample dependence within the experimental error. This is seen in Fig. 3, which plots the full-width at half-maximum, FWHM, of $\partial R_H/\partial B_2$ isotherms (Fig. 1(b)), and in Fig. 4, which depicts the crossover field, B_0 , extracted from the fits to $R_H(B_2)$ for a range of low temperatures in the temperature-magnetic field phase diagram.

To corroborate this fundamental finding, we have carried out two additional measurements. The standard single-field Hall-effect setup is used to monitor the differential Hall coefficient \tilde{R}_H as a function of the magnetic field B_1 applied along the crystallographic c axis (see Supplementary Information I). In addition, the magnetoresistivity, ρ , is measured as a function of a single field, B_2 , applied within the ab plane. Both $\rho(B_2)$ and $\tilde{R}_H(B_1)$ can similarly be decomposed into background and critical terms (see Supplementary Information IV), with the critical crossover terms occurring near the basal-plane critical field, B_{2c} , and near the c -axis critical field, B_{1c} , respectively; the ratio B_{2c}/B_{1c} will be used as the anisotropy ratio to convert the B_1 scale into an equivalent B_2 . The zero-field and high-field values extracted from fits of the crossover function (eq. 5) to magnetoresistivity (ρ^0 and ρ^∞) and differential Hall coefficient (\tilde{R}_H^0 and \tilde{R}_H^∞) are presented in Fig. 2(b) and in Fig. S7 of the Supplementary Information, respectively. Each quantity shows a similar sample dependence: As found for the crossed-field results, the differences $\rho^0 - \rho^\infty$ and $\tilde{R}_H^0 - \tilde{R}_H^\infty$ remain finite in the zero-temperature limit even though the individual quantities differ for the different samples. The crossover positions extracted from all the properties are compiled in Fig. 4. They are largely compatible with each other, falling within a range spanned by the FWHM; they de-

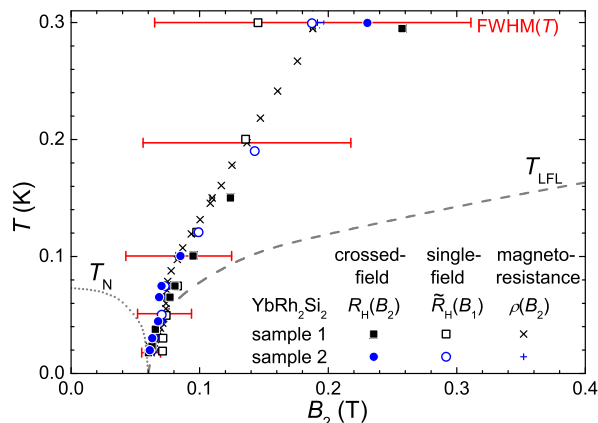


Fig. 4. Position of the Hall crossover in the temperature-field phase diagram of YbRh_2Si_2 . The crossover fields, B_0 , are extracted from fits to $R_H(B_2)$ of the crossed-field experiment, to $\tilde{R}_H(B_1)$ of the single-field experiment, and to $\rho(B_2)$ (cf. Methods). The values of the single-field Hall-effect experiment were scaled by 1/11 to account for the magnetic anisotropy of YbRh_2Si_2 . The red horizontal bars reflect the FWHM at selected temperatures determined by the fit in Fig. 3 showing that the crossover fields of the various experiments and samples all lie within the range spanned by the FWHM. The dotted (dashed) line represents the boundary of the antiferromagnetic phase (Fermi liquid regime) taken from Ref. [13]. Error bars are omitted in order to avoid confusion with the width of the crossover; with the exception of the data at 0.3 K and the single-field result of sample 2 at 0.19 K the standard deviations are smaller than the symbol size.

fine a crossover energy scale (the T^* -line) [14, 20]. Finally, the FWHM of the crossover in $\tilde{R}_H(B_1)$ and $\rho(B_2)$ closely follow that of $R_H(B_2)$ (see Fig. 3). We note that the onset of the quadratic form of $R_H^0(T)$ at T_N (Fig. 2) is not accompanied by a similar signature in the FWHM at T_N (Fig. 3, see Supplementary Information IV and V). Therefore, the FWHM extrapolates to zero for $T \rightarrow 0$ implying a jump of all three quantities ($R_H(B_2)$, $\tilde{R}_H(B_1)$ and $\rho(B_2)$) at the QCP.

The sample independence of both the crossover position and the crossover FWHM strongly indicates that all the magnetotransport crossovers manifest the same underlying physics. Combined with the jump of the Hall coefficient and magnetoresistivity in the zero-temperature limit, they imply the interpretation in terms of a sharp Fermi-surface reconstruction at the magnetic QCP [14] over that based on the smooth physics of heavy quasiparticles [15, 17].

Having isolated the critical component of the Hall crossover from the background term, we are now in the position to discuss the detailed nature of the QCP. For this purpose, we have not only carried out crossed-field and single-field Hall and (single-field) magnetoresistivity measurements over an extended field range for each temperature, but have also done so for a large set of temperatures in the low- T range. These efforts allow us to reach the important and entirely new conclusion that the crossover FWHM is proportional to temperature (Fig. 3).

The Fermi surface is a property of the single-electron excitation spectrum. In any Fermi liquid, it spans the momenta, \mathbf{k}_F , at which the energy dependence of the single-electron Green's function develops a pole at the Fermi energy. Hence, a reconstruction of the Fermi surface across the QCP implies that the single-electron Green's function contains a singularity at the QCP. Indeed, the conduction-electron Green's function of a Kondo lattice system can very generally be written as

$$G(\mathbf{k}, E, T) = \frac{1}{E - \epsilon_{\mathbf{k}} - \Sigma(\mathbf{k}, E, T)}. \quad [1]$$

In the absence of static Kondo screening, the self-energy $\Sigma(\mathbf{k}, E, T)$ is non-singular. Correspondingly, the Fermi surface is smoothly connected to that of the conduction electrons alone; it is small [22]. In the presence of static Kondo screening, $\Sigma(\mathbf{k}, E)$ develops a pole; for E and T small compared to the coherent Kondo scale, it takes the form

$$\Sigma(\mathbf{k}, E, T) = \frac{(v^*)^2}{E - \epsilon_f^*} + \Delta\Sigma(\mathbf{k}, E, T). \quad [2]$$

Here v^* and ϵ_f^* specify the strength and energy of the Kondo resonance [21], and $\Delta\Sigma(\mathbf{k}, E, T)$ is the non-singular term of the self-energy. The existence of this pole in $\Sigma(\mathbf{k}, E, T)$ shifts the Fermi momenta from their positions on the small Fermi surface, \mathbf{k}_F , to those on a large Fermi surface, \mathbf{k}_F^* . Approaching the point of critically-destroyed Kondo effect, the quasiparticle weight vanishes [6, 7] in accordance with the divergence of the quasiparticle mass seen in specific heat and resistivity [13, 22]. In particular, at the QCP, both the strength, v^* , and the energy, ϵ_f^* , of the Kondo resonance (see eq. 2) go to zero in the $E \rightarrow 0$ and $T \rightarrow 0$ limit. Moreover, the interacting nature of the fixed point implies an E/T -scaling of the single-electron Green's function: the reasoning is analogous to that for the dynamical spin susceptibility [6, 9], and the property can be illustrated by explicit calculations in simplified model settings for critical Kondo destruction [23]. Similar forms of dynamical scaling of the single-electron spectra are likely a generic feature of other types of Kondo-destroying QCPs [7, 8, 24]; they appear in related contexts as well [25, 26, 27]. It is worth noting that the linear-in-temperature electrical resistivity cannot be used as evidence for E/T -scaling of the

single-electron excitations. Indeed, the temperature dependence of the electrical resistivity does not in general measure the temperature dependence of the single-electron relaxation rate and this is so even for spin-density-wave QCPs [28].

The scaling form for the single-electron Green's function in the quantum-critical regime can be expressed as follows:

$$G(\mathbf{k}_F, E, T) \sim \frac{1}{T^\alpha} g(\mathbf{k}_F, \frac{E}{T}). \quad [3]$$

The associated relaxation rate, defined in the quantum relaxation regime ($E \ll k_B T$) according to

$$\Gamma(\mathbf{k}_F, T) \equiv [-i\partial \ln G(\mathbf{k}_F, E, T)/\partial E]_{E=0}^{-1}, \quad [4]$$

is linear in temperature: $\Gamma(\mathbf{k}_F, T) = cT$, where c is a universal constant.

Discussion

We can use these properties of the single-electron Green's function to understand the crossover of the Hall coefficient. In the Fermi-liquid regimes on either side of the QCP, the Hall coefficient reflects the respective Fermi surface; it is in particular independent of the quasiparticle residue [29] (see Supplementary Information VI). The distinct (large and small) Fermi surfaces in the two Fermi-liquid regimes yield different end values of the Hall coefficient. The central question is how the two Fermi surfaces are connected across the QCP. Because the single-electron Green's function characterizes each of the two Fermi liquids, this is related to the critical relaxation rate, $\Gamma(\mathbf{k}_F, T)$, of the single-electron states. At zero temperature, $\Gamma(\mathbf{k}_F, T = 0)$ vanishes; the change from one Fermi surface to the other is sharp, occurring precisely at the QCP. The Hall coefficient must undergo a sharp jump in accordance with the experimental findings. At any non-zero temperature, a continuous crossover from one Fermi surface to the other is controlled by the single-electron relaxation rate $\Gamma(\mathbf{k}_F, T)$. Given the above described behavior of the Hall coefficient in the adjacent Fermi-liquid regimes with well defined but different Fermi surfaces, its crossover has to be related to the finite-temperature broadening of the critical single-electron states on the Fermi surface. Our observation of a linear-in-temperature width of the critical Hall crossover is therefore consistent with a linear-in-temperature relaxation rate. By contrast, our experimental finding is incompatible with the spin-density-wave picture of order parameter fluctuations and the concomitant Gaussian fixed point, which would be accompanied by a superlinear temperature dependence of the Hall crossover width (see section VI of the Supplementary Information).

The single-electron Green's function serves as the proper means to specify whether a metal obeys the standard theory of solids - Landau's Fermi-liquid theory. The fact that eq. (3), with a non-zero v^* , *i.e.*, a large Fermi surface across the QCP, fails to describe our data is consistent with a breakdown of the heavy-Fermi-liquid quasiparticles at the QCP. More generally

eq. (3), reminiscent of the Green's function of gapless interacting electrons in one dimension [30], invalidates any Fermi-liquid description. By using a single set of measurements on the same compound to probe both the collective fluctuations of the QCP and a critical destruction of the single-electron excitations, our work provides the most direct association between quantum criticality and non-Fermi-liquid behavior.

In summary, we have carried out in-depth magnetotransport measurements in a prototypical quantum critical heavy-fermion metal, and we are able to distinguish a robust critical crossover from a sample-dependent background feature. By zooming into the vicinity of the QCP, we have shown that the width of the critical crossover is not only independent of sample quality but also proportional to temperature. This proportionality is consistent with the E/T form in the dynamical critical scaling. Coupled with the fact that the vanishing width in the zero-temperature limit implies a jump in the Fermi surface, our findings point to the microscopic many-body excitations of a collapsing Fermi surface as underlying the dynamical E/T -scaling of the macroscopic critical fluctuations. Our results further establish the T^* -line as a means to probe the Kondo breakdown. This should hold even when the Kondo breakdown is separated from the paramagnetic-to-antiferromagnetic QCP [31]. In addition, they might help to understand why the two coincide in stoichiometric YbRh₂Si₂ and its close vicinity. More generally, the linkage between microscopics and macroscopics is expected to be broadly relevant to the physics of strong correlations, considering that the finite-temperature properties are invariably abnormal in a wide array of quantum materials, and given that the Fermi surface and its evolution as a function of control parameters - *e.g.* from the underdoped high-temperature cuprate superconductors to the overdoped ones [32, 33] - are playing an increasingly central role in understanding these systems.

Materials and Methods

The Hall crossovers in both the crossed-field ($R_H(B_2)$) and single-field ($\tilde{R}_H(B_1)$) experiments (see Supplementary Information I) were fitted with the empirical crossover function

$$R_H(B) = R_H^\infty + mB - \frac{R_H^\infty - R_H^0}{1 + (B/B_0)^p} \quad [5]$$

that contains not only a critical component [14] but also a linear term mB to account for the background behavior. R_H^0 and R_H^∞ are the zero-field and infinite-field values, respectively. The differential Hall coefficient and the magnetoresistivity curves were analyzed analogously leading to the corresponding parameters \tilde{R}_H^0 , \tilde{R}_H^∞ and ρ^0 , ρ^∞ , respectively. By fitting eq. 5 to isotherms taken at different temperatures, the temperature dependences of the parameters were extracted. The FWHM was extracted from the derivative of the fitted function as illustrated in the inset of Fig. 1.

ACKNOWLEDGMENTS. We acknowledge discussions with P. Gegenwart, A. Rosch, and A. Schofield. Part of the work at Dresden was supported by the DFG Research Unit 960 "Quantum Phase Transitions". S. P. acknowledges funding from the European Research Council under the European Community's Seventh Framework Programme (FP7/2007-2013)/ERC grant agreement n° 227378. S. K. and Q. S. were supported by the NSF and the Welch Foundation Grant No. C-1411.

1. Nature Physics focus issue. Quantum phase transitions. *Nature Phys* 4, 167-204 (2008).
2. Ma, S-K *Modern Theory of Critical Phenomena* (Addison-Wesley, Redwood, 1976).
3. Hertz, J A *Quantum Critical Phenomena*. *Phys Rev B* 14, 1165-1184 (1976).
4. Millis, A J Effect of a nonzero temperature on quantum critical-points in itinerant fermion systems. *Phys Rev B* 48, 7183-7196 (1993).
5. Sachdev, S *Quantum Phase Transitions* (Cambridge Univ Press, Cambridge, 1999).
6. Si, Q, Rabello, S, Ingersent, K & Smith, J.L Locally critical quantum phase transitions in strongly correlated metals. *Nature* 413, 804-808 (2001).

7. Coleman, P, Pépin, C, Si, Q & Ramazashvili, R How do Fermi liquids get heavy and die? *J Phys: Condens Matter* 13, R723-R738 (2001).
8. Senthil, T, Vojta, M & Sachdev, S Weak magnetism and non-Fermi liquids near heavy-fermion critical points. *Phys Rev B* 69, 035111 (2004).
9. Schröder, A et al. Onset of antiferromagnetism in heavy-fermion metals. *Nature* 407, 351-355 (2000).
10. Aronson, M C et al. Non-Fermi-liquid scaling of the magnetic response in $UCu_{5-x}Pd_x$ ($x = 1, 1.5$). *Phys Rev Lett* 75, 725-728 (1995).

11. Stockert, O et al. Magnetic Fluctuations at a Field-Induced Quantum Phase Transition. *Phys Rev Lett* 99, 237203 (2007).
12. Trovarelli, O et al. YbRh_2Si_2 : Pronounced non-Fermi-liquid effects above a low-lying magnetic phase transition. *Phys Rev Lett* 85, 626–629 (2000).
13. Gegenwart, P et al. Magnetic-field induced quantum critical point in YbRh_2Si_2 . *Phys Rev Lett* 89, 056402 (2002).
14. Paschen, S et al. Hall effect evolution at a heavy fermion quantum critical point. *Nature* 432, 881–885 (2004).
15. Norman, M R Hall number in YbRh_2Si_2 . *Phys Rev B* 71, 220405(R) (2005).
16. Löhneysen, H v, Rosch, A, Vojta, M & Wölfle, P Fermi-liquid instabilities at magnetic quantum phase transitions. *Rev Mod Phys* 79, 1015–1075 (2007).
17. Rourke, P M C et al. Magnetic-Field Dependence of the YbRh_2Si_2 Fermi Surface. *Phys Rev Lett* 101, 237205 (2008).
18. Friedemann, S et al. Band-structure and anomalous contributions to the Hall effect of YbRh_2Si_2 . *Physica B* 403, 1251–1253 (2008).
19. Friedemann, S et al. Hall effect measurements and electronic structure calculations on YbRh_2Si_2 and its reference compounds LuRh_2Si_2 and YbIr_2Si_2 . *Phys Rev B* in the press (2010).
20. Gegenwart, P et al. Multiple energy scales at a quantum critical point. *Science* 315, 969–971 (2007).
21. Coleman, P Heavy Fermions: electrons at the edge of magnetism. *Handbook of Magnetism and Advanced Magnetic Materials* (J Wiley and Sons) Vol. 1, edited by H Kronmüller and S Parkin, Vol. 1, 95–148 (2007).
22. Gegenwart, P, Si, Q & Steglich, F Quantum criticality in heavy-fermion metals. *Nature Phys* 4 186–197 (2008).
23. Zhu, L, Kirchner, S, Si, Q & Georges, A Quantum critical properties of the Bose-Fermi Kondo Model in a large-N limit. *Phys Rev Lett* 93, 267201 (2004).
24. Paul, I, Pépin, C & Norman, M R Kondo breakdown and hybridization fluctuations in the Kondo-Heisenberg lattice. *Phys Rev Lett* 98, 026402 (2007).
25. Varma, C M, Littlewood, P B, Schmitt-Rink, S, Abrahams, E & Ruckenstein, A E Phenomenology of the normal state of Cu-O high temperature superconductors. *Phys Rev Lett* 63, 1996–1999 (1989).
26. Anderson, P W The 'strange metal' is a projected Fermi liquid with edge singularities. *Nature Phys* 2, 626–630 (2006).
27. Senthil, T Critical Fermi surfaces and non-Fermi liquid metals. *Phys Rev B* 78, 035103 (2008).
28. Rosch, A Magnetotransport in nearly antiferromagnetic metals. *Phys Rev B* 62, 4945–4962 (2000).
29. Khodas, M & Finkel'stein, A M Hall coefficient in an interacting electron gas. *Phys Rev B* 68, 155114 (2003).
30. Orgad, D Spectral functions for the Tomonaga-Luttinger and Luther-Emery Liquids. *Philos Mag B* 81, 377–398 (2001).
31. Friedemann, S et al. Detaching the antiferromagnetic quantum critical point from the Fermi surface reconstruction in YbRh_2Si_2 . *Nature Phys* 5, 465–469 (2009).
32. Doiron-Leyraud, N et al. Quantum oscillations and the Fermi surface in an underdoped high- T_c superconductor. *Nature* 447, 565–568 (2007).
33. Vignolle, B et al. Quantum oscillations in an overdoped high- T_c superconductor. *Nature* 455, 952–955 (2008).

Supplementary Information for “Fermi-surface collapse and dynamical scaling near a quantum critical point”

Sven Friedemann¹, Niels Oeschler¹, Steffen Wirth¹, Cornelius Krellner¹, Christoph Geibel¹, Frank Steglich¹, Silke Paschen², Stefan Kirchner^{3,4}, Qimiao Si³

¹ Max Planck Institute for Chemical Physics of Solids, Nöthnitzer Str. 40, 01187 Dresden, Germany ² Institute of Solid State Physics, TU Vienna, Wiedner Hauptstr. 8-10, 1040 Vienna, Austria ³Department of Physics and Astronomy, Rice University, Houston, Texas 77005-1892, USA ⁴ Max Planck Institute for the Physics of Complex Systems, Nöthnitzer Str. 38, 01187 Dresden, Germany

Experimental Details

For the low-temperature Hall effect and magnetoresistivity measurements, a dilution refrigerator was utilized ($T \geq 18$ mK). A solenoid along with a split-coil magnet allowed for Hall effect measurements in the crossed-field geometry which is sketched in Fig. S6(a). In this setup the dual role of the magnetic field is unraveled by using one field (B_1) to generate the Hall response and another field (B_2) to tune the ground state of the sample across the quantum critical point.

The small magnetic field (B_1) provided by the solenoid is used to produce the linear-response Hall effect. Therefore it was oriented along the magnetic hard c axis and perpendicular to the electrical current flowing within the crystallographic ab plane. Consequently, the Hall voltage V_y is generated transverse to the current within the ab plane. The induced voltages were amplified by low-temperature transformers and the signals were measured by a standard lock-in technique. We extracted the Hall resistivity ρ_H as the anti-symmetric component of the field-reversed transversal voltage, $\rho_H(B_1, B_2) = t[V_y(+B_1, B_2) - V_y(-B_1, B_2)]/2I$ (with t being the thickness of the sample). The linear-response Hall coefficient $R_H(B_2)$ was subsequently derived from the initial slope of the Hall resistivity $\rho_H(B_1, B_2)|_{B_2}$

$$R_H(B_2) \equiv \lim_{B_1 \rightarrow 0} \rho_H(B_1, B_2)/B_1 \quad [\text{S6}]$$

for small fields $B_1 \leq 0.4$ T (cf. Fig. S5).

The split-coil magnet generating the tuning field which tunes the material from the magnetic ground state to the paramagnetic one is applied within the magnetic ab plane. This magnet covers a range of B_2 extending to a value as large as 4 T, nearly two orders of magnitude larger than the ab -plane critical field, $B_{2c} \approx 0.06$ T. The combination of the two magnets and the dilution refrigerator enabled us to access a wide range of both temperature and magnetic field. This was essential for extracting the temperature dependence of the FWHM as well as for the separation of the crossover and background contributions. The fitting of the isotherms was restricted to below 2 T for the crossed-field Hall results due

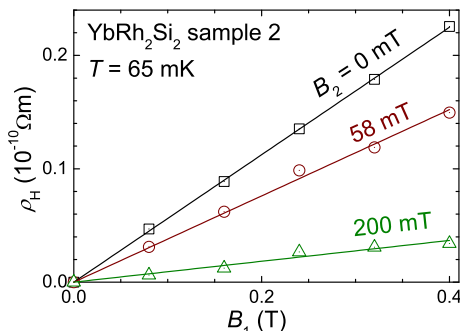


Fig. S5. Calculation of the initial-slope Hall coefficient. The figure shows typical isotherms of the Hall resistivity $\rho_H(B_1, B_2)$ at selected fields B_2 . The solid lines herein are linear fits to the data used to calculate the linear-response Hall coefficient, $R_H(B_2) = \rho_H(B_1, B_2)/B_1$.

to deviations from linearity at higher fields. These deviations are likely associated with the Zeeman-splitting of the bands, which becomes sizable in this field range since B_2 is applied in the easy magnetic plane.

In the case of the single-field Hall experiment ($B_2 = 0$) (see Fig. S6(b)), the differential Hall coefficient

$$\tilde{R}_H(B_1) \equiv \frac{\partial \rho_H(B_1, 0)}{\partial B_1} \quad [\text{S7}]$$

was calculated and analyzed. The fitting of the differential Hall coefficient $\tilde{R}_H(B_1)$ with eq. 3 of the main text leads to the parameters \tilde{R}_H^0 and \tilde{R}_H^∞ . In the case of the single-field Hall experiment, the fitting was performed over the full field range up to 4 T.

Special care was spent to a precise alignment of the field B_1 to be parallel to the c axis within less than 0.5° . Such precise alignment is essential for the single-field experiment as a small component of this field within the ab plane could easily dominate the tuning due to the large magnetic anisotropy of the material.

The magnetoresistivity $\rho(B_2)$ (see Fig. S6(c) for a sketch of the setup) was monitored during the crossed-field Hall-effect measurements. By an analogous fitting with the crossover function the corresponding parameters ρ^0 and ρ^∞ were extracted. We note that for the magnetoresistivity curves the linear term mB is negligibly small (cf. section S6).

Samples

Single crystals of YbRh_2Si_2 were synthesized using an indium flux-growth technique as described earlier [1]. An additional optimization of the initial composition and the temperature profile led to an improved sample quality. This is manifested in an almost doubled residual resistance ratio of sample 2 (RRR = 120) compared to sample 1 (RRR = 70). All samples were polished to thin ($t \lesssim 80 \mu\text{m}$) platelets and prescreened via resistivity $\rho(T, B)$ measurements to ensure indium-free samples.

Two different samples are considered. Sample 1 was taken from Ref. [2] and remeasured in the newly designed high-resolution setup applying the precise alignment procedure described in section as a cross check. Sample 2 was chosen from our highest quality batch (see above). These two samples span the whole range of sample dependences in the low-temperature Hall effect [3]: the low-temperature Hall coefficient seems to depend on tiny changes of the composition (samples from the same batch, on the other hand, show identical behavior).

Anomalous Hall contribution

In heavy-fermion metals, an asymmetric scattering of the conduction electrons from the $4f$ moments – the skew scattering – leads to an anomalous contribution to the Hall coefficient mostly relevant at high temperatures [4]. However, our analysis of the crossover at the quantum critical point (QCP) is not

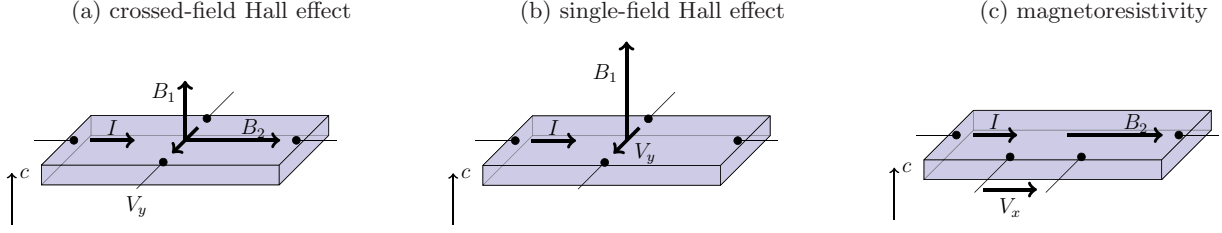


Fig. S6. Experimental setups. The experimental setups of the crossed-field and single-field Hall effect and of the magnetoresistivity measurements are depicted (from left to right).

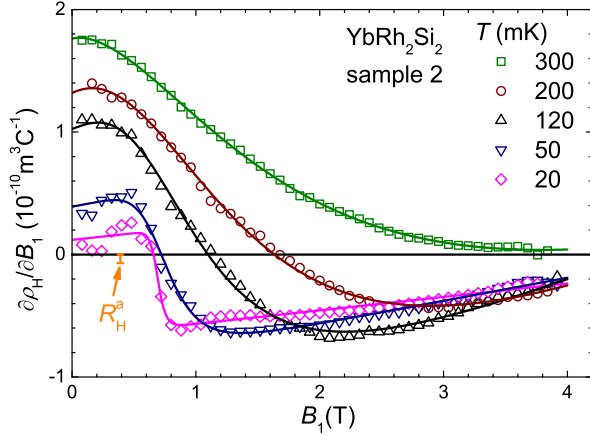


Fig. S7. Single-field results on sample 2 of YbRh_2Si_2 . Selected isotherms of the numerically derived differential Hall coefficient $\tilde{R}_H(B_1) = \partial\rho_H/\partial B_1$ for sample 2 are plotted against B_1 . The solid lines are fits of the crossover function (see methods section of the main text). At large fields $B \gg B_0$, the third term of eq. 3 of the main text becomes negligible. Consequently, the Hall resistivity is expected to be described by the integral of the first two terms ($\tilde{R}_H^\infty + mB_1$), i.e. $\rho_H = c + \tilde{R}_H^\infty B_1 + \frac{m}{2} B_1^2$ with c denoting the intercept with the ordinate, $\rho_H(B_1 = 0)$. This form was consistently fitted. The vertical, orange bar represents the anomalous contribution determined from eq. S8 via the derivative $R_H^a = \partial\rho_H^a/\partial B_1$ (see text).

affected by the anomalous Hall effect, since its contribution to the Hall resistivity

$$\rho_H^a(B_1) = C\rho(B_1)\mu_0 M(B_1) \quad [\text{S8}]$$

is essentially linear in field. It adds a small, but constant anomalous contribution R_H^a to the differential Hall coefficient with an absolute value of less than $0.07 \times 10^{-10} \text{ m}^3/\text{C}$. This is negligible compared to the large variation of $\partial\rho_H/\partial B_1$ (compare vertical bars in Fig. S7 and Fig. S10(b)). Furthermore, both the inflection point and the sharpness of the crossover are invariant to a constant offset. In eq. S8, C denotes a constant which was determined from fits to $R_H(T)$ at high temperatures ($\approx 100 \text{ K}$ in YbRh_2Si_2) [5] where no sample dependences are observed [3]. The resistivity $\rho(B_1)$ was measured simultaneously, and the magnetization $M(B_1)$ for the relevant geometry ($B \parallel c$) was taken from Ref. [6]. Since the anomalous contribution does not influence our analysis, we have simply considered the raw data.

Crossovers in Hall effect and magnetoresistivity

Figure S7 shows the single-field Hall-effect results of YbRh_2Si_2 for sample 2. The crossover found in the differential Hall coefficient $\tilde{R}_H(B_1)$ was fitted by the same crossover function as in the crossed-field experiment (eq. 3 of the main text). In particular, it is possible to identify the crossover and background contributions. The corresponding results and the fits

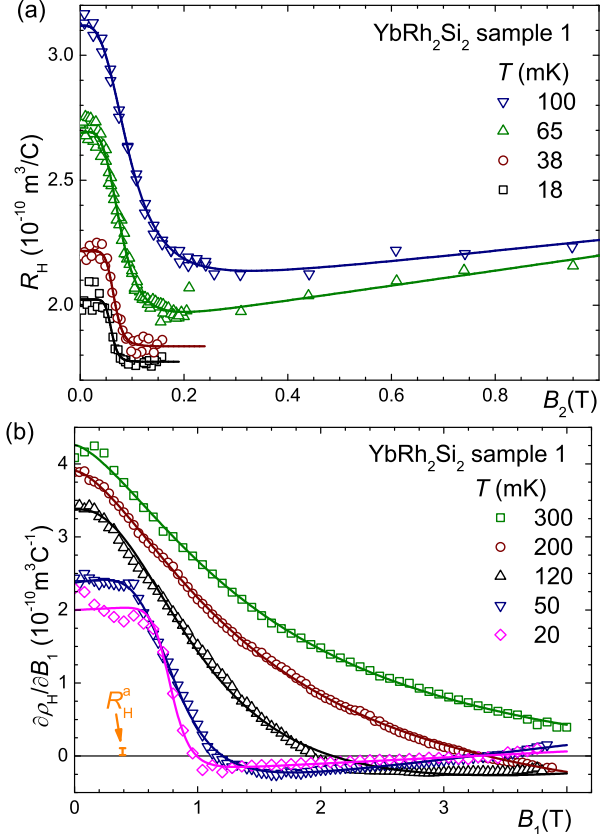


Fig. S8. Hall effect results on sample 1 of YbRh_2Si_2 . (a) Crossed-field and (b) single-field results for the Hall coefficient $R_H(B_2)$ and the differential Hall coefficient $\tilde{R}_H(B_1)$, respectively. For a description of the fitting function we refer to the Methods section of the main text. As in Fig. S7, the anomalous contribution R_H^a is indicated by the vertical, orange bar (see also section).

for the crossed-field ($R_H(B_2)$) and the single-field ($\tilde{R}_H(B_1)$) experiments of sample 1 are shown in Fig. S8.

The magnetoresistivity ($\rho(B_2)$) data are illustrated in Fig. S9 for sample 1 and 2. Here, the same crossover function (eq. 3 of the main text) was used, with the linear term being negligibly small, $m \simeq 0$. We analyzed the magnetoresistivity crossover up to 1 K. This allows us to extract the FWHM over this enlarged temperature range as depicted in Fig. S10 proving that the width follows the unique linear temperature up to such high temperatures.

No signature is seen in the temperature dependence of the FWHM for any of the experiments at the Néel transition (cf. main text). Only below 30 mK does the FWHM extracted from both the crossed-field Hall effect and the magnetoresistivity crossovers seem to tend slightly towards larger values compared to the overall linear temperature dependence, see

Fig. 3 of the main text. We assign this to influences arising from the nearby classical phase transition as at this temperature the phase boundary is approached by the Hall crossover. This is seen in the phase diagram with the FWHM around the crossover field substantially extending into the magnetically ordered phase for temperatures below 30 mK only (cf. horizontal bars in Fig. 4 of the main text), the temperature

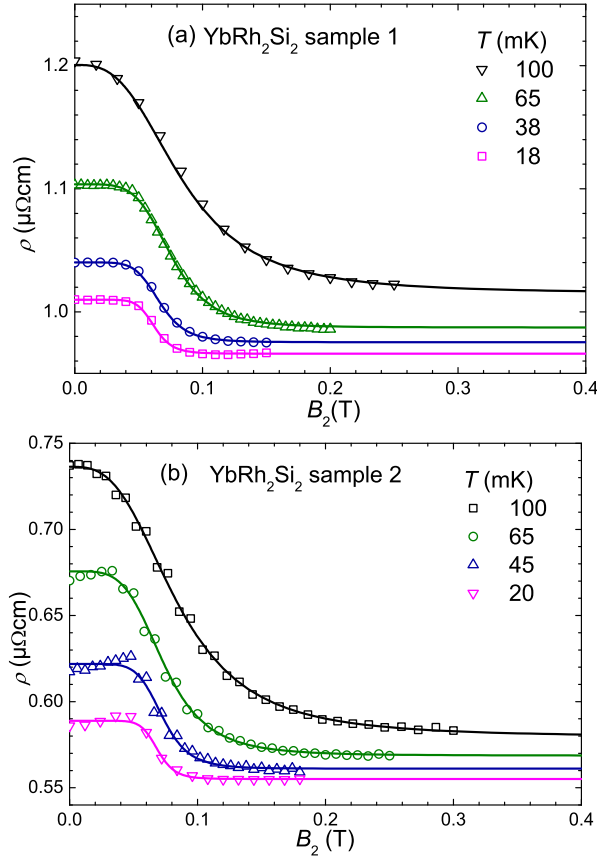


Fig. S9. Crossover in the magnetoresistivity $\rho(B_2)$ of YbRh_2Si_2 . Results (a) for sample 1 and (b) for sample 2 are depicted. The data were measured simultaneously with the crossed-field Hall effect experiment. For the fitting of the crossover (eq. 3 of the main text) the linear background term was omitted.

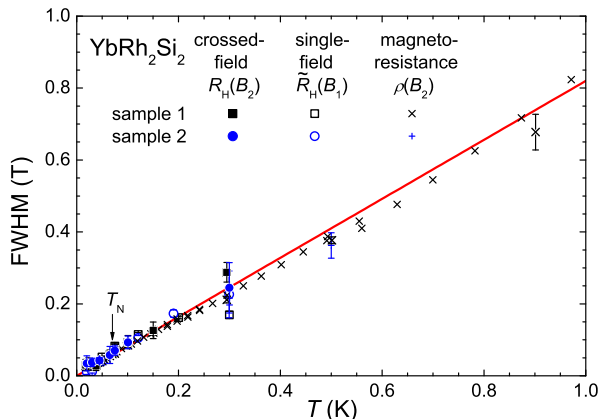


Fig. S10. Full-width at half-maximum (FWHM) up to 1 K. The results extracted from the magnetoresistivity crossover are depicted in an enlarged temperature range up to 1 K. Solid line represents the very same linear fit as in Fig. 3 of the main text. It is referred to Fig. 3 of the main text for further explanations.

below which the seeming deviations from linearity occur. Further indications of this additional influence are observed in the crossed-field Hall coefficient curves which exhibit visible spread at lowest temperatures within the ordered phase (Fig. 1 of the main text and Fig. S10).

The FWHM extracted from the single-field measurements on the other hand continues to obey the linear form down to the lowest temperatures accessed. Given this continuity, we consider the single-field data to represent the intrinsic quantum critical behavior. This property of the single-field experiment may arise from the fact that only here the tuning-field is applied along the magnetic hard axis. For this orientation the magnetization and consequently also the classical magnetic fluctuations are by almost one order of magnitude smaller compared to those for fields applied within the magnetic easy plane [6]. The latter configuration is realized in both the crossed-field Hall effect and the magnetoresistivity measurements.

Finally, we would like to note that within the experimental accuracy the FWHM of all the measurements is compatible with the linear form in the whole temperature range. Taking all this together, the data imply that the linear temperature

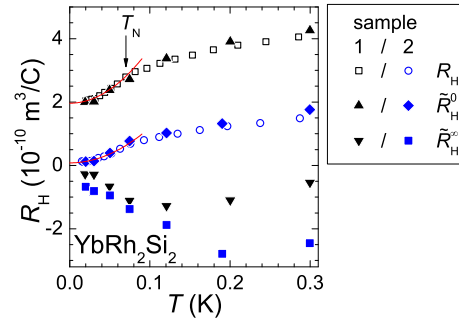


Fig. S11. Limiting values of the single-field Hall crossover. Fit parameters \tilde{R}_H^0 and \tilde{R}_H^∞ of the single-field Hall-effect measurement $\tilde{R}_H(B_1)$. Results for sample 1 and sample 2 are depicted along with initial-slope Hall coefficient. Solid curves represent quadratic fits as discussed in the text (see also Fig. S12). Standard deviations are smaller than the symbol size.

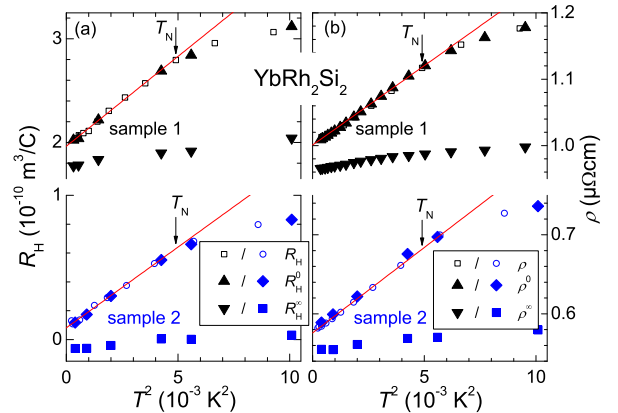


Fig. S12. Evolution of the Hall coefficient in the antiferromagnetically ordered phase. (a) Initial-slope Hall coefficient $R_H(T)$ is plotted against T^2 together with the fit parameters R_H^0 and R_H^∞ . Solid lines represent fits of the form $R_H(T) = c + A'T^2$ for temperatures below T_N (indicated by arrows) where c denotes the intercept with the ordinate, i.e. the zero-temperature Hall coefficient, $R_H(T = 0)$. These fits are reproduced as solid curves in Fig. 2(a) of the main text and in Fig. S11. (b) Corresponding plot of the resistivity $\rho(T)$ and the fit parameters ρ^0 and ρ^∞ extracted from the magnetoresistivity crossover with an according fitting function $\rho(T) = \rho_0 + AT^2$ (ρ_0 being the residual resistivity) below T_N which agrees well with previous observations [6].

dependence of the FWHM represents the behavior intrinsic to the quantum criticality.

The vanishing FWHM implies a jump of the magnetoresistivity at zero temperature, in contrast to the common behavior of Kondo systems for which the width of the change in magnetoresistivity remains finite at zero temperature [7]. This represents a key element in our interpretation of the Hall crossover in terms of a Fermi-surface reconstruction.

Sample dependence of the background contribution

The temperature dependences of R_H^0 and R_H^∞ are shown in Fig. 2(a) of the main text for both samples. The results of the low-field value R_H^0 are in good agreement with those of the measured zero-field ($B_2 = 0$) initial-slope Hall coefficient $R_H(T)$ (Ref. [3]). This is non-trivial as R_H^0 is the result of the fitting procedure specified in the Methods section of the main text, and not fixed to the zero-field value. Both, $R_H^0(T)$ and $R_H^\infty(T)$ decrease as the temperature decreases. Below T_N , the Hall coefficient clearly obeys a quadratic temperature dependence as demonstrated in Fig. S12(a). This finding allows for a proper extrapolation of $R_H(T)$ and $R_H^0(T)$ to $T \rightarrow 0$ which in turn enables us to conclude that the difference between R_H^0 and R_H^∞ , *i.e.* the height of the Hall crossover, remains finite for both samples on approaching zero temperature. Identical observations were made for the parameters extracted from the magnetoresistivity crossover (Fig. S12(b) and Fig. 2(b) of the main text) as well as for those of the crossover in the single-field Hall effect (Fig. S11).

The temperature evolution of the parameter m of eq. 3 of the main text (which describes the linear background) is shown in Fig. S13 for all Hall-effect experiments. The data for the single-field experiments are restricted to below 0.2 K due to the crossover extending over an increasingly large field range with increasing temperature. This prevents a proper determination of the background contribution within the field range of our experiment (cf. Fig. S7 and Fig. S8(b)). The crossed-field results of sample 1 are limited to temperatures above 0.065 K due to a lack of high-field data at lower T (cf. Fig. S8(a)).

Taking all these together we find a pronounced sample dependence for the quantities describing the background contribution whereas those associated with the critical crossover are essentially sample independent (cf. main text).

Single-electron Green's function and the Hall crossover

The single-electron Green's function, $G(\mathbf{k}, E, T)$ (eq. 1 of the main text) on either side of the zero-temperature transition and at low temperatures, can be decomposed as

$$G(\mathbf{k}, E, T) = G_{\text{coh}}(\mathbf{k}, E, T) + G_{\text{inc}}(\mathbf{k}, E, T). \quad [\text{S9}]$$

This decomposition is an immediate consequence of the fact that the phases separated by the QCP are taken to be Fermi liquids. Indeed, because of the jump of the Hall coefficient across the QCP, the Fermi liquids are taken to have large and small Fermi surfaces, respectively. The coherent part of $G(\mathbf{k}, E, T)$ is given by

$$G_{\text{coh}}(\mathbf{k}, E, T) = \frac{z_{\mathbf{k}}}{E - \varepsilon(\mathbf{k}) + i\Gamma_{\mathbf{k}}(T)} \quad [\text{S10}]$$

describing a quasiparticle, and $G_{\text{inc}}(\mathbf{k}, E, T)$ is a background contribution. The strength of the quasiparticle excitation, $z_{\mathbf{k}}$, formally defined as the residue of the pole, is non-zero in either phase. However, to be compatible with the continuous nature of the zero-temperature transition, $z_{\mathbf{k}}$ must vanish as the QCP is approached: $z_{\mathbf{k}} \rightarrow 0$ as $B \rightarrow B_c$. At $T = 0$, the quasiparticle damping $\Gamma_{\mathbf{k}}$ vanishes at the small Fermi-momenta \mathbf{k}_F

for $B < B_c$, and at the large Fermi-momenta \mathbf{k}_F^* for $B > B_c$; at these respective Fermi-momenta, the quasiparticles become infinitely-sharp excitations at zero temperature. The coherent part of $G(\mathbf{k}, E, T)$ is therefore the diagnostic feature on either side of the transition, and it jumps at the QCP in accord with the sudden Fermi surface change.

This jump is manifested in the Hall measurement, because the Hall coefficient is independent of the quasiparticle residue. Note that our argument builds on the Landau Fermi-liquid nature of the phases on either side of the QCP, where the Fermi surface and the forms (S9) and (S10) are well defined. The Hall coefficient of a Fermi liquid is completely determined by the dispersion of the single-electron excitations near the Fermi surface [8, 9]. The fact that the quasiparticle residue does not appear in the Hall coefficient of a Fermi liquid can be seen in a number of related ways. It is known – both phenomenologically [10] and microscopically [11] – that the Boltzmann equation of a Fermi liquid does not depend on the quasiparticle residue; by extension, the Hall coefficient does not depend on the quasiparticle residue. The same conclusion is reached through a study of the Hall coefficient of a Fermi liquid using the Kubo formula [8]. Finally, for a spherically symmetric but otherwise arbitrary dispersion it has been shown explicitly by diagrammatic calculations that the Hall coefficient is not renormalized by the electron-electron interactions [9].

At non-zero temperatures, the quasiparticle relaxation rate at either \mathbf{k}_F for $B < B_c$, or \mathbf{k}_F^* for $B > B_c$, no longer vanishes. In fact, inside the Fermi-liquid phase (with either large or small Fermi surface), the temperature dependence of $\Gamma_{\mathbf{k}_F}$ has to be quadratic in T . However, the Fermi surface remains well defined in these regimes. At finite temperatures, the change from one Fermi surface to the other is therefore restricted to the intermediate quantum critical regime. Because of the absence of a phase transition at any non-zero temperature, the sharp reconstruction of the Fermi surface at $T = 0$ is turned into a Fermi-surface crossover across the $T^*(B)$ line. The restriction to the quantum critical regime implicates that the linear in temperature relaxation rate present in this regime determines the broadening of the Fermi surface change. From the relation of the Hall coefficient to the Fermi surface (described above) we associate the width of the Hall crossover with this broadening and consequently with the relaxation rate Γ of the single-electron Green's function.

To be more specific, consider a general scaling form for the single-electron Green's function at the Fermi momentum in the quantum critical region:

$$G(E, T) = \frac{1}{T^\alpha} \phi\left(\frac{E}{T^x}\right). \quad [\text{S11}]$$

For a Gaussian fixed point, a dangerously irrelevant variable will invalidate E/T -scaling and make $x > 1$. Correspondingly, the single-particle relaxation rate Γ (defined in eq. 4 of the main text) will be superlinear in temperature and the Hall crossover width as a function of the magnetic field will in general not be linear in temperature. An interacting fixed point, on the other hand, can generate $x = 1$ with a relaxation rate that is linear in temperature and be compatible with the linear-in- T Hall-crossover width observed.

An important question concerns the critical exponent y as defined by the $T^*(B)$ line, $T^*(B) \propto (B - B_c)^y$. This scale equivalently specifies $B^*(T)$, the center of the critical Hall crossover. In general, B^* and FWHM are two independent parameters. Eq. 5, which fits our data very well (Figs. 1, S3, S4, S5), invokes both parameters to characterize the critical component of the Hall crossover. We have already shown that the FWHM is robustly linear in temperature. For the $T^*(B)$

line, Fig. 4 of the main text suggests that the exponent y is less than 1 but its precise determination, especially from the Hall-effect measurements, requires accuracies beyond our present experiments.

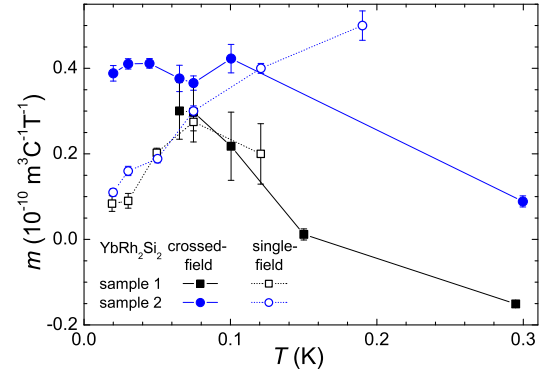


Fig. S13. Temperature dependence of m , the slope of the linear background contribution extracted from the crossed-field and single-field Hall-effect measurements.

1. Trovarelli, O et al. YbRh_2Si_2 : Pronounced non-Fermi-liquid effects above a low-lying magnetic phase transition. *Phys Rev Lett* 85, 626–629 (2000).
2. Ref. 14 of main text: Paschen, S et al. Hall effect evolution at a heavy fermion quantum critical point. *Nature* 432, 881–885 (2004).
3. Ref. 18 of main text: Friedemann, S et al. Band-structure and anomalous contributions to the Hall effect of YbRh_2Si_2 . *Physica B* 403, 1251–1253 (2008).
4. Fert, A and Levy, P M Theory of the Hall effect in heavy-fermion compounds. *Phys Rev B* 36 1907–1916 (1987)
5. Paschen, S et al. Anomalous Hall effect in YbRh_2Si_2 . *Physica B* 359, 44–46 (2005).
6. Ref. 13 of main text: Gegenwart, P et al. Magnetic-field induced quantum critical point in YbRh_2Si_2 . *Phys Rev Lett* 89, 056402 (2002).
7. Schlottmann, P Bethe-Ansatz solution of the ground-state of the SU (2j+1) Kondo (Coqblin-Schrieffer) model: Magnetization, magnetoresistance and universality. *Z Phys B: Condens Matter* 51, 223–235 (1983).
8. Kohno, H & Yamada, K A General Expression for Hall Coefficient Based on Fermi Liquid Theory. *Prog Theor Phys* 80, 623–643 (1998).
9. Ref. 29 of main text: Khodas, M & Finkel'stein, A M Hall coefficient in an interacting electron gas. *Phys Rev B* 68, 155114 (2003).
10. Pines, D & Noziere, P *The Theory of Quantum Liquids*, vol. I. Perseus (1999).
11. Betbeder-Matibet, O & Nozieres, P Transport equation for quasiparticles in a system of interacting fermions colliding on dilute impurities. *Ann Phys* 37 17–54 (1966).

